Received: 8 November 2021 | Revised: 17 January 2022 | Accepted: 20 January 2022

DOI: 10.1002/nag.3339

RESEARCH ARTICLE

WILEY

An Arbitrary Lagrangian Eulerian (ALE) finite difference (FD)-SPH depth integrated model for pore pressure evolution on landslides over erodible terrains

Manuel Pastor[1] | **Saeid M. Tayyebi**[1] | **Miguel M. Stickle**[1] | **Miguel Molinos**[1] | **Angel Yague**[2] | **Diego Manzanal**[2] | **Pedro Navas**[2]

[1] Mathematics and Computer Science Applied to Civil and Naval Engineering, ETS Ingenieros de Caminos, Universidad Politécnica de Madrid, Madrid, Spain

[2] Department of Continuum Mechanics and Structures, ETS Ingenieros de Caminos, Universidad Politécnica de Madrid, Madrid, Spain

Correspondence
Manuel Pastor, Mathematics and Computer Science Applied to Civil and Naval Engineering, ETS Ingenieros de Caminos, Universidad Politécnica de Madrid, Madrid, Spain.
Email: manuel.pastor@upm.es

Funding information
MINECO, Grant/Award Number: P-LAND (PID2019-105630GB-I00)

Abstract

Entrainment of saturated bed material increases the mobility of fast landslides. The distribution of excess pore pressures changes in the body of the landslide, as the material entering it has much lower effective confining stresses which results on much smaller apparent basal friction angles. The purpose of this paper is to enhance the Finite Differences depth integrated SPH model developed by the authors to cope with material which is flowing up the FD meshes. The model is set within an Arbitrary Lagrangian Eulerian framework (ALE), and the resulting excess pore pressure evolution model will include now advective terms in addition to the diffusive and source terms. In order to assess the importance of the proposed modification, we introduce a basal Péclet number which relates two non dimensional reference times of consolidation and erosion.

KEYWORDS

ALE, coupled, depth integrated, entrainment, excess pore pressure, SPH

1 | INTRODUCTION

Fast landslides cause every year severe economic damage and loss of lives around the world. In order to minimize their impact, it is necessary to estimate their risk using suitable modelling tools able to reproduce the fundamental aspects of these phenomena such as the triggering conditions, the mass involved, the velocity of propagation, depth, runout, and geometry of the final deposit, and the forces of the landslide on buildings and structures.

To this purpose, a great effort has been devoted by researchers to develop such models, proposing innovative mathematical, constitutive and rheological, and numerical models.

Two important aspects contributing to increase velocities and runout of the landslides are (i) pore pressure evolution both within the flowing mass and the basal materials and (ii) entrainment of bed material, which increases the mass. In depth integrated models, the former contribute to change the apparent friction angle at the bottom of the landslide. Liquefaction is a limit case where the frictional component of the basal friction approaches zero.

The role of pore pressure has been studied since 1971,[1] when Hutchinson and Bandari showed how undrained loading was a fundamental mechanism both in the inception and propagation phases. Later, Hutchinson,[2] proposed a simple 1 block sliding-consolidation model. Further development is due to Iverson[3] and Iverson and Denlinger.[4] Later, Pastor et al.,[5,6] introduced 1D models which were coupled to the nodes of SPH depth integrated models. These 1D models were

discretized using simple lagrangian finite differences (FD) schemes. The nodes kept a fixed relative position in the soil columns associated to each node.

Regarding erosion, properties of the entrained material influence the overall behaviour of the flowing mass, modifying its mobility, specially in cases where bed materials were saturated, with excess pore pressures induced by the landslide. Abele[7] pointed out the role of the mobilization of bed saturated materials a mechanism increasing the mobility of landslides such as rockslides. The role of undrained loading and the pore pressures induced in the bed has been studied by Sassa et al.[8,9]

When modelling erosion within the framework of depth integrated models, we have to be aware of the existence of the correcting terms described by Iverson et al.,[10,11] Le and Pitman,[12] and Pudasaini and Fisher.[13]

Most of proposed models for landslide propagation have been so far depth integrated models, including a specific submodel which predicts the erosion rate. The situation is changing, as full 3D models are being developed. It is worth mentioning the pioneering work of Crosta et al.,[14] where a Finite Element Arbitrary Lagrangian Eulerian (ALE) model was used to describe both landslide and bed induced entrainment, and the more recent of Nikooeis and Manzari[15] where the SPH technique has been used.

There exist a great variety of basal erosion laws. The interested reader is addressed to Iverson and Ouyang, where laws proposed by researchers such as Takahashi,[16] Egashira et al.,[17] Fraccarollo and Capart,[18] Pitman et al.,[19] or McDougall and Hungr[20] are described.

One important aspect in snow and some submarine avalanches is ploughing at the front, which contributes to modifying both the velocity and entrainment of the bed material (see, for instance, the work of Issler et al.[21] and Issler.[22])

The entrainment of saturated bed materials with excess pore water pressures can increase the mass and the mobility of fast landslides. The key question is how this phenomenon can be modelized in depth integrated models, where the vertical structure of the flow has been lost.

A possible solution could consist of using FD meshes associated to landslide nodes. But, in some cases, an error would be introduced as the material flows through the mesh as a consequence of the erosion process. The 1D model for the columns should not be of lagrangian but ALE type.

The main objectives of this paper are:

i. To describe how to extend the 1D Lagrangian model proposed by Pastor et al.[5,6] to include the material movement across the FD meshes. We propose here a 1D ALE scheme which includes advective, diffusive and source terms. The relative strength of the advective part to the diffusive terms of the PDE describing excess pore pressure variations is important.
ii. In order to assess whether the proposed approach is or is not necessary, we propose using a Péclet non dimensional number that characterizes the relative strengths of advection and diffusion. Should this Péclet number be much lower than unity, it will not be necessary to use the proposed ALE model, the classical approach being valid.

Therefore, our purpose is not to introduce a novel erosion model nor to compare a set of the many models available today. Indeed, we will use the simple model proposed by McDougall and Hungr[20] to describe the rate of erosion. The proposed methodology will be valid for other more complex laws.

The paper is organized as follows. First, we present the general two phase, coupled, depth integrated model proposed by Pastor et al.[5,6] Then, Section 3 is devoted to describing the problem of entrainment of saturated bed materials, where the domain changes along time incorporated the entrained material. The problem is of Stefan type with a condition to be applied at the mobile boundary. We will describe the problem using an ALE model. The mathematical nature of the problem changes, becoming an advection-diffusion type of problem. We will introduce two characteristic non dimensional times for consolidation and erosion and a non dimensional number, the basal entrainment Péclet number describing the relative importance of advective and diffusive terms. Section 4 is devoted to presenting two examples, one to illustrate the influence of the proposed Péclet number, the second presenting a debris flow case which happened in Hong Kong in 1990.

2 | TWO PHASE, COUPLED, DEPTH INTEGRATED MODELLING FRAMEWORK

2.1 | Introduction

We will recall here for completeness the two phases general depth integrated model including pore water evolution along depth presented in Pastor et al.[6] The model is a generalization of the models developed by the authors in the past years for

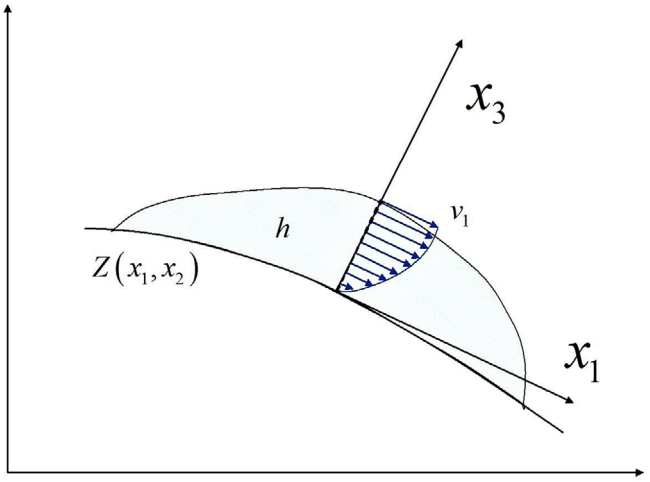

FIGURE 1 Reference system, coordinates and notation used in the analysis

one phase materials[9,39] with a refined description of pore water pressure evolution along depth and debris flows where no pore water pressures were taken into account.[23]

From the general model, all other mentioned models can be derived, as they are particular cases of it. Moreover, when using the general model for debris flows with very high permeability, we recover the two phase debris flow model with no pore water pressure. If we make the permeability very small and include pore pressure evolution, we obtain the one phase model with coupled pore pressures.

2.2 | Models for depth integrated fast landslides on two phase saturated soils

The depth integrated model can be obtained from the models developed in the past by Biot[24] and Zienkiewicz and his group at Swansea University.[25] Similar results were proposed in the area of granular media by Anderson and Jackson.[26] Pitman and Le[27] and Pudasaini[28] have proposed depth integrated two phase models for debris flows. It is worth mentioning the work of Córdoba et al.[29] who have applied the Pitman and Le model to debris flow propagation, and Bui and co-workers[30] who have recently proposed a 3D SPH model for geomechanical problems incorporating two separate phases.

Depth integrated models have been—and still are—extensively used for ocean, coastal, harbour and hydraulics engineering problems. They are useful simplifications of the much more computing time demanding 3D models, providing a good compromise between cost and accuracy. This type of models was introduced by Saint Venant in 1871.[31] In the case of avalanche dynamics, Savage and Hutter[32,33] proposed their much celebrated 1D Lagrangian model, where a simple Mohr-Coulomb model allowed a description of the granular material behaviour. This work was extended to 2D and more complex terrains in Hutter et al.,[34] Gray et al.[35] It has been applied by Laigle and Coussot,[36] McDougall and Hungr,[37] Pastor et al.[38,39] and Quecedo et al.[40] Concerning limitations of the model, Hutter et al.[41] provide a detailed discussion, being worth mentioning the textbook by Pudasaini and Hutter.[42]

The reference system is that sketched in Figure 1, where Z denotes the basal surface elevation and h the depth of the flowing mass.

Velocities will be denoted as $\{v_1, v_2, v_3\}$, and sub-indexes s and w will refer to solid and fluid phases.

An over bar over a magnitude indicates it is a depth averaged value. For instance:

$$\bar{\theta} = \frac{1}{h}\int_{Z}^{Z+h} \theta(x_1, x_2, x_3)\, dx_3 \tag{1}$$

The main variables and magnitudes used in the analysis are:

i. The porosity n (volume fraction of voids in the mixture).

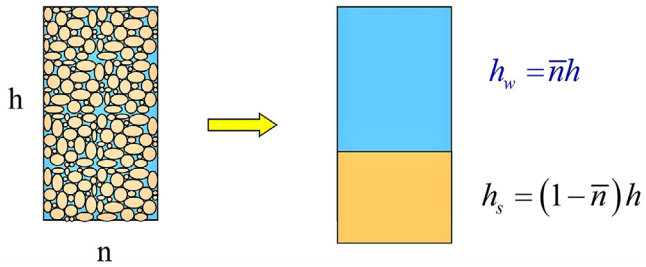

FIGURE 2 Definition of auxiliary variables h_s and h_w

ii. The phase densities, defined as:

$$\rho^{(s)} = (1-n)\rho_s$$
$$\rho^{(w)} = n\rho_w \tag{2}$$

where ρ_s and ρ_w are the densities of solid particles and the pore fluid.

iii. The material derivatives relative to solid and fluid are given by:

$$\frac{d^{(s)}}{dt} = \frac{\partial}{\partial t} + \boldsymbol{v_s}^T.\text{grad}$$
$$\frac{d^{(w)}}{dt} = \frac{\partial}{\partial t} + \boldsymbol{v_w}^T.\text{grad} \tag{3}$$

where $\boldsymbol{v_s}$ and $\boldsymbol{v_w}$ are the velocities of soil and pore fluid. They are related by :

$$\frac{d^{(w)}}{dt} = \frac{d^{(s)}}{dt} + (\boldsymbol{v_w} - \boldsymbol{v_s})^T.\text{grad} \tag{4}$$

Above relation can be casted in terms of the Darcy's velocity $\boldsymbol{w}$ used in Soil Mechanics:

$$\boldsymbol{v_w} = \boldsymbol{v_s} + \frac{\boldsymbol{w}}{n} \tag{5}$$

iv. We will use the following depth averaged velocities:

$$\bar{n},\ \bar{\boldsymbol{v}}_s,\ \bar{\boldsymbol{v}}_w,\ \bar{\boldsymbol{v}} = (1-\bar{n})\bar{\boldsymbol{v}}_s + \bar{n}\ \bar{\boldsymbol{v}}_w \tag{6}$$

and the 'quasi material derivative':

$$\frac{\bar{d}}{dt} = \frac{\partial}{\partial t} + \bar{\boldsymbol{v}}_j \frac{\partial}{\partial x_j} \qquad j = 1,2 \tag{7}$$

v. We will define, for convenience, two auxiliary variables h_s and h_w which characterize the solid and fluid contents in a column of water of height h (Figure 2).

$$h = h_s + h_w$$
$$h_s = (1-\bar{n})h \quad h_w = \bar{n}h \tag{8}$$

Depth integrated equations are obtained by applying Leibnitz's rule to the 3D equations of the balance of mass and linear momentum:

1. Balance of mass equations, we obtain:

$$\begin{aligned}\frac{\bar{d}^{(s)}}{dt}((1-\bar{n})h) + (1-\bar{n})h\,\mathrm{div}\,\bar{\boldsymbol{v}}_{\boldsymbol{s}} &= (1-\bar{n})\,e_R\\ \frac{\bar{d}^{(w)}}{dt}(\bar{n}\,h) + \bar{n}\,h\,\mathrm{div}\,\bar{\boldsymbol{v}}_{\boldsymbol{w}} &= \bar{n}\,e_R\end{aligned} \tag{9}$$

where e_R is the erosion rate, defined as the increment of height of the moving soil per unit time. We have assumed that the porosity of the erodible bed is the same as that of the avalanche. If not so, the terms of porosity on the RHS should be $(1-\bar{n}_b)\,e_R$ and $\bar{n}_b e_R$, $\bar{n}_b$ being the porosity of the bed material.

2. The balance of momentum equations are:

$$\begin{aligned}\rho_s h_s \frac{\bar{d}^{(s)}\bar{\boldsymbol{v}}_{\boldsymbol{s}}}{dt} = \mathrm{grad}\left\{\frac{1}{2}(1-\bar{n})\rho_s h^2 b_3\right\} &+ \mathrm{grad}(\bar{n}\,h\,\Delta\bar{p}_w)\\ &+ \frac{1}{2}\rho_w h^2 b_3\,\mathrm{grad}\,\bar{n} - h\,\Delta\bar{p}_w\mathrm{grad}\,\bar{n}\\ &- \boldsymbol{\tau}_{\boldsymbol{b}}^{(s)} + \rho_s \boldsymbol{b} h_s + h_s\,\bar{\boldsymbol{R}}_s - (1-\bar{n})\rho_s\left(\bar{\boldsymbol{v}}_{\boldsymbol{s}} - \bar{\boldsymbol{v}}_s{}^{(b)}\right)e_R\end{aligned} \tag{10}$$

for the solid, and

$$\begin{aligned}\rho_w h_w \frac{d^{(w)}\bar{\boldsymbol{v}}_{\boldsymbol{w}}}{dt} = \mathrm{grad}\left\{\frac{1}{2}\bar{n}\rho_w h^2 b_3\right\} &- \mathrm{grad}(\bar{n}\,h\,\Delta\bar{p}_w)\\ &- \frac{1}{2}\rho_w h^2 b_3\,\mathrm{grad}\,\bar{n} + h\,\Delta\bar{p}_w\mathrm{grad}\,\bar{n}\\ &- \boldsymbol{\tau}_{\boldsymbol{b}}^{(w)} + \rho_w \boldsymbol{b} h_w + h_w\,\bar{\boldsymbol{R}}_w - \bar{n}\,\rho_w\left(\bar{\boldsymbol{v}}_{\boldsymbol{w}} - \bar{\boldsymbol{v}}_w{}^{(b)}\right)e_R\end{aligned} \tag{11}$$

for the fluid. We have assumed that the stresses are hydrostatic. In above equations:

i. b_3 is the component of the body forces (gravity) along x_3.
ii. The depth averaged pore pressure $\bar{p}_w$ will be decomposed into a hydrostatic part and an excess pore pressure as:

$$\bar{p}_w = \bar{p}_{w,hydr} + \Delta\bar{p}_w \tag{12}$$

iii. The interaction between solid and fluid phases is given by the terms $\bar{\boldsymbol{R}}_s$ and $\bar{\boldsymbol{R}}_w$.
iv. We have assumed a certain amount of slip on the base, characterized by $\bar{\boldsymbol{v}}_s^{(b)}$and $\bar{\boldsymbol{v}}_w^{(b)}$, as proposed by Iverson.[11]
v. We have introduced the shear basal stresses of the solid and fluid phases as:

$$\boldsymbol{\tau}_{\boldsymbol{b}\boldsymbol{i}}^{(s)} = \quad -\sigma_{i3}^{(s)}\Big|_Z \qquad \boldsymbol{\tau}_{\boldsymbol{b}\boldsymbol{i}}^{(w)} = \quad -\sigma_{i3}^{(w)}\Big|_Z \tag{13}$$

where $-\sigma_{i3}^{(s)}|_Z$, and $-\sigma_{i3}^{(w)}|_Z$ are the stresses of the solid and water phases at the bottom.

This model, proposed by Pastor et al.,[6] reduces to the model proposed by Pitman and Le[27] just by assuming that excess pore pressures $\Delta\bar{p}_w$ are zero. The model has to be completed with descriptions of the basal shear stresses and the interaction forces between phases.

Looking at the balance of mass and momentum equations for both phases, they can be added, which results on:

$$\frac{\bar{d}^{(s)}}{dt}((1-\bar{n})h) + \frac{\bar{d}^{(w)}}{dt}(\bar{n}\,h) + (1-\bar{n})h\,\mathrm{div}\,\bar{\boldsymbol{v}}_{\boldsymbol{s}} + \bar{n}\,h\,\mathrm{div}\,\bar{\boldsymbol{v}}_{\boldsymbol{w}} = (1-\bar{n})\,e_R + \bar{n}\,e_R \tag{14}$$

and

$$\begin{aligned}\rho_s h_s \frac{\bar{d}^{(s)}\bar{\boldsymbol{v}}_{\boldsymbol{s}}}{dt} + \rho_w h_w \frac{d^{(w)}\bar{\boldsymbol{v}}_{\boldsymbol{w}}}{dt} &= \text{grad}\left\{\frac{1}{2}(1-\bar{n})\rho_s h^2 b_3\right\} + \text{grad}\left\{\frac{1}{2}\bar{n}\rho_w h^2 b_3\right\} \\ &+ \text{grad}(\bar{n}\, h\, \Delta\bar{p}_w) - \text{grad}(\bar{n}\, h\, \Delta\bar{p}_w) \\ &+ \frac{1}{2}\rho_w h^2 b_3 \,\text{grad}\,\bar{n} - \frac{1}{2}\rho_w h^2 b_3 \,\text{grad}\,\bar{n} \\ &- h\,\Delta\bar{p}_w \text{grad}\,\bar{n} + h\,\Delta\bar{p}_w \text{grad}\,\bar{n} \\ &- \boldsymbol{\tau}_{\boldsymbol{b}}^{(s)} - \boldsymbol{\tau}_{\boldsymbol{b}}^{(w)} \\ &+ \rho_s \boldsymbol{b} h_s + \rho_w \boldsymbol{b} h_w \\ &+ h_s \bar{\boldsymbol{R}}_{\boldsymbol{s}} + h_w \bar{\boldsymbol{R}}_{\boldsymbol{w}} \\ &- (1-\bar{n})\rho_s\left(\bar{\boldsymbol{v}}_{\boldsymbol{s}} - \bar{\boldsymbol{v}}_s^{(b)}\right)e_R - \bar{n}\,\rho_w\left(\bar{\boldsymbol{v}}_{\boldsymbol{w}} - \bar{\boldsymbol{v}}_w^{(b)}\right)e_R\end{aligned} \tag{15}$$

If the velocities of soil and water and their material derivatives are such that:

$$\frac{\bar{d}^{(s)}\bar{\boldsymbol{v}}_{\boldsymbol{s}}}{dt} = \frac{d^{(w)}\bar{\boldsymbol{v}}_{\boldsymbol{w}}}{dt} \tag{16}$$

and the gradients of porosity are neglected, the LHS result:

$$\begin{aligned}&\frac{\bar{d}\,h}{dt}\,\text{div}\,\bar{\boldsymbol{v}} + h\,\text{div}\,\bar{\boldsymbol{v}} \quad \text{and} \\ &\rho h \frac{\bar{d}\,\bar{\boldsymbol{v}}}{dt}\end{aligned} \tag{17}$$

where $\bar{\rho} = (1-\bar{n})\rho_s + \bar{n}\rho_w$ is the mixture density, and $\boldsymbol{v} = \boldsymbol{v}_{\boldsymbol{s}} = \boldsymbol{v}_{\boldsymbol{w}}$.

The equations reduce to those of a one phase material:

$$\begin{aligned}&\frac{\bar{d}\,h}{dt} + h\,\text{div}\,\bar{\boldsymbol{v}} = e_R \\ &\bar{\rho} h \frac{\bar{d}\,\bar{v}}{dt} = \text{grad}\left\{\frac{1}{2}\bar{n}\rho h^2 b_3\right\} - \boldsymbol{\tau}_{\boldsymbol{b}} + \bar{\rho}\boldsymbol{b}h - \bar{\rho}\left(\bar{\boldsymbol{v}} - \bar{\boldsymbol{v}}^{(b)}\right)e_R\end{aligned} \tag{18}$$

It is interesting to note that the pore water pressure does not appear explicitly in the above equations, but it influences the basal friction term.

For convenience, from now on, we will drop the over bar, all magnitudes being depth integrated unless otherwise stated.

3 | PORE WATER PRESSURE EVOLUTION: AN ALE BASED FD SCHEME FOR LANDSLIDES PROPAGATION OVER AN ERODIBLE BED

3.1 | Classical approach

Regarding the pore water pressure evolution, we will recall the expressions given in Pastor et al.[5,6]:

$$\begin{aligned}\frac{d^{(s)}\Delta p_w}{dt} &= -\bar{\rho}' b_3 \frac{d^{(s)}h}{dt}\left(1 - \frac{x_3}{h}\right) \\ &+ \frac{K_v}{\alpha}\frac{\partial}{\partial x_3}\left(\frac{\bar{n}}{\bar{C}_d}\frac{\partial \Delta p_w}{\partial x_3}\right) - \frac{K_v}{\alpha}\frac{1}{1-\bar{n}}\frac{d^{(s)}\bar{n}}{dt}\end{aligned} \tag{19}$$

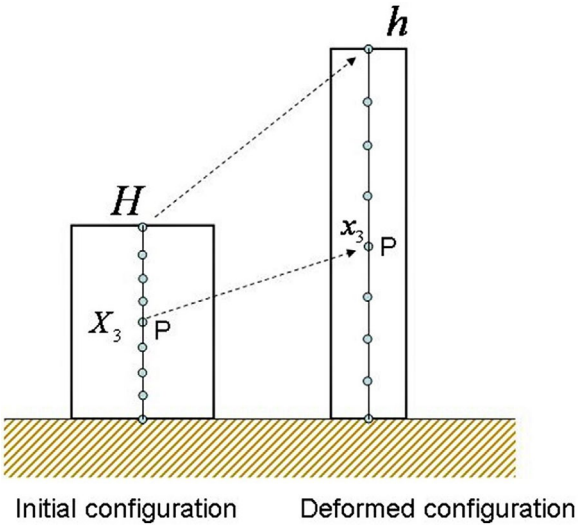

FIGURE 3 Deformation of a column of soils. Note that grid nodes are material points

where we have introduced the effective density $\bar{\rho}' = \bar{\rho} - \rho_w$. $K_v = \frac{E}{3(1-2\nu)}$ is the volumetric stiffness of soil skeleton,E the Young's modulus, ν the Poisson's ratio, α being a constitutive parameter, such that when the state of stress is purely hydrostatic, then $\alpha = 1$, while under a state of stress $(k_0\sigma_1,\ k_0\,\sigma_1, \sigma_3)$ $\alpha = k_0$.

In above equation, $\bar{C}_d = \frac{C_d}{n}$ with $\boldsymbol{R} = C_d\,(v_w - v_s)$.

R is the interaction solid-fluid force:

$$\boldsymbol{R} = -n\boldsymbol{R_w} = (1-n)\boldsymbol{R_s} \tag{20}$$

and the coefficient C_d depends on the interaction force. For instance, for a Darcy flow, R is given by:

$$\boldsymbol{R} = n{k_w}^{-1} w = C_d\,(v_w - v_s) \tag{21}$$

where k_w is the permeability tensor. Other alternatives, such as that used by Pitman and Le[27] (see Anderson and Jackson[26]), can be used for a wider range of porosities, and when the relative velocity is larger:

$$\boldsymbol{R} = \frac{n(1-n)}{V_T n^m}(\rho_s - \rho_w)g(v_w - v_s) \tag{22}$$

where V_T is the terminal velocity of solid particles falling in the fluid, g the acceleration of gravity and m a constant. The coefficient C_d can be obtained as:

$$C_d = \frac{n(1-n)}{V_T n^m}(\rho_s - \rho_w)g \quad \left(\text{Anderson and Jackson}^{26}\right) \tag{23}$$

It is a parabolic PDE which, in addition to the diffusive term $\frac{K_v}{\alpha}\frac{\partial}{\partial x_3}\left(\frac{n}{\bar{C}_d}\ \frac{\partial \Delta p_w}{\partial x_3}\right)$, includes two source terms:

i. $-\rho' b_3 \frac{d^{(s)}h}{dt}\left(1 - \frac{x_3}{h}\right)$, the increment of excess pore pressure caused by an increase of the debris flow height.

ii. $-\frac{K_v}{\alpha}\frac{1}{1-\bar{n}}\frac{d^{(s)}\bar{n}}{dt}$, the changes of excess pwp caused by changes of porosity.

This equation can be discretized using an explicit FD scheme based on the Lagrangian grid depicted in Figure 3. In the models proposed by Pastor et al.,[5,6] the SPH technique was used to discretize the balance of mass and momentum equations. Associated to every SPH node of solid a FD grid was introduced.

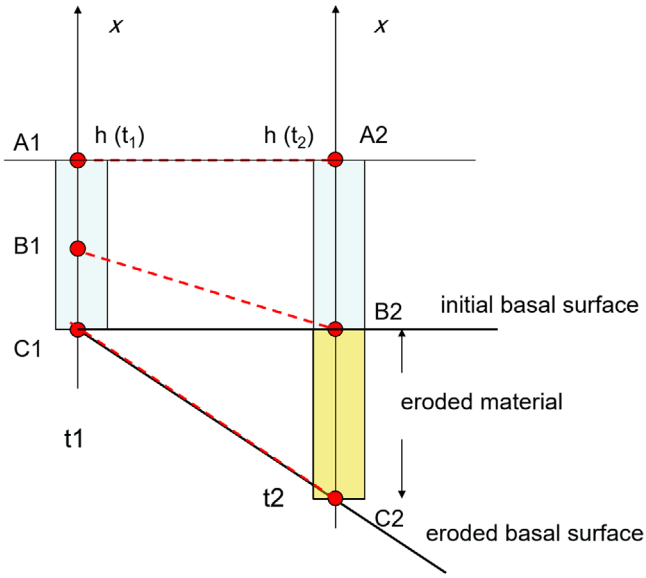

FIGURE 4 Proposed Arbitrary Lagrangian Eulerian (ALE) grid

Let us consider the LHS term, $\frac{d^{(s)}\Delta p_w}{dt}$, of Equation (19) which is a material derivative following the solid particles along x_3. The nodes of the finite element grid move with the material, which means that derivatives with respect to time following a particular node are material derivatives coinciding with partial derivatives. Therefore, the discretization of this term at a time n and a point j of the grid can be approximated by the forwards difference:

$$\left.\frac{d^{(s)}\Delta p_w}{dt}\right|_j^n = \left.\frac{\partial}{\partial t}\Delta p_w\right|_j^n = \frac{\Delta p_w|_j^{n+1} - \Delta p_w|_j^n}{\Delta t} \tag{24}$$

where the partial derivative $\frac{\partial}{\partial t}\Delta p_w|_j^n$ represents the rate of change at node j - because it moves with the material. It is important to notice that this formulation is no longer valid if the material moves with respect to the mesh.

The number and position of the nodes of the FD grid depend on the type of problem. We used 11 FD nodes (10 subdivisions) for most problems. The boundary conditions were:

i. On the top boundary, the excess pore water pressure was usually assumed to be zero.
ii. On the bottom, if the landslide was flowing over an impermeable base, the flow was assumed to be zero. In the case of mitigation structures such as basal grids (see Tayyebi et al.[43]), we assumed the bottom layer to be at atmospheric pressure.

Regarding the initial conditions, we assumed linear profiles with a value at the basal surface ranging from 0 to the pressure causing liquefaction of the material.

3.2 | PWP modelling in landslides over erodible terrain

In the preceding section, we have described a Lagrangian formulation which can be used provided no material is being entrained in the landslide. Otherwise, the formulation is not correct, the magnitude of the error being dependent on the erosion rate.

Let us consider the evolution of the column of soil sketched in Figure 4 For the sake of simplicity, we have used x as the vertical axis. The velocity of the material along x is denoted as u, and depends only on time if we disregard the change of h caused by the divergence of the horizontal velocity. We will not consider either the effect of porosity.

The 1D mathematical model simplifies to:

$$\frac{d^{(s)}\Delta p_w}{dt} = \frac{K_v}{\alpha}\frac{\partial}{\partial x}\left(\frac{\bar{n}}{\bar{C}_d}\frac{\partial \Delta p_w}{\partial x}\right) \quad 0 \le x \le h(t) \tag{25}$$

where Δp_w will depend on x and t. Introducing the coefficient of consolidation:

$$C_v = \frac{K_v}{\alpha}\frac{\bar{n}}{\bar{C}_d} \tag{26}$$

The equation can be written as:

$$\frac{d^{(s)}\Delta p_w}{dt} = C_v \frac{\partial^2 \Delta p_w}{\partial x^2} \tag{27}$$

which is the classical 1D consolidation equation. To solve the model, we will have to add two boundary conditions and the initial condition.

Note that the equation is defined in the variable domain $0 \le x \le h(t)$, with boundary conditions applied both to the top and the bottom. It is, therefore, a Stefan problem (Crank,[44] and Hill[45]), with the condition:

$$\frac{dh}{dt} = e_R \tag{28}$$

which relates the rates of erosion and the change of height h.

In order to discretize it, there are two main approaches: (i) enlarge the mesh adding new nodes with the entrained material,[46] and (ii) use the same mesh with nodes which are moving to keep their relative position in the mesh.[47] This is illustrated in Figure 4, where we have considered a column of soil at time t1, which increases its length as erosion is taking place. Let us consider three representative nodes along x, A, B and C, located at the top, middle height and bottom of the column. Node C, at time 1, has a material different from what it has at time 2, node C2. Node B, located at the middle of the column at time 1, will have eroded material below it.

The material velocity u of any point of the column will be constant and equal to the erosion rate e_R. The velocity at which nodes are moving is:

$$w = \frac{x}{h}\frac{dh}{dt} = e_R\frac{x}{h} \tag{29}$$

The relative velocity is therefore given by the difference $u - w$:

$$u - w = e_R\left(1 - \frac{x}{h}\right) \tag{30}$$

When the consolidation equation is discretized, the material derivative can then be related to the partial derivative with respect to a moving node of the mesh j as:

$$\left.\frac{d^{(s)}}{dt}\Delta p_w\right|_j^n = \left.\frac{\partial \Delta p_w}{\partial t}\right|_j^n + (u - w)\left.\frac{\partial \Delta p_w}{\partial x}\right|_j^n \tag{31}$$

This equation embraces two limit cases:

i. Static reference mesh, for which $w = 0$

$$\left.\frac{d^{(s)}}{dt}\Delta p_w\right|_j^n = \left.\frac{\partial \Delta p_w}{\partial t}\right|_j^n + u\left.\frac{\partial \Delta p_w}{\partial x}\right|_j^n \tag{32}$$

which is the material derivative, and

ii. mesh with nodes moving with the particles, for which $u = w$ and

$$\left.\frac{d^{(s)}}{dt}\Delta p_w\right|_j^n = \left.\frac{\partial \Delta p_w}{\partial t}\right|_j^n \tag{33}$$

In the case we are considering, taking into account Equation 30:

$$\left.\frac{d^{(s)}}{dt}\Delta p_w\right|_j^n = \left.\frac{\partial \Delta p_w}{\partial t}\right|_j^n + e_R\left(1-\frac{x}{h}\right)\left.\frac{\partial \Delta p_w}{\partial x}\right|_j^n \tag{34}$$

and the consolidation equation will result on the described grid on:

$$\left.\frac{\partial \Delta p_w}{\partial t}\right|_j^n + e_R\left(1-\frac{x}{h}\right)\left.\frac{\partial \Delta p_w}{\partial x}\right|_j^n = C_v\left.\frac{\partial^2 \Delta p_w}{\partial x^2}\right|_j^n \tag{35}$$

This equation can be written combines advection and diffusive terms. The equation is of the type:

$$\frac{\partial \phi}{\partial t} + A\frac{\partial \phi}{\partial x} = D\frac{\partial^2 \phi}{\partial x^2} \tag{36}$$

where A and D characterize the advection and diffusion parts. In our case, A depends on the position, being zero at the top of the column where $x = h$.

If we introduce a characteristic length l, the Peclet number characterizes the relative influence of both phenomena:

$$P_e = \frac{A.l}{D} \tag{37}$$

Large values of P_e correspond to advection dominated flows, while very small values indicate diffusive problems where advection has little importance.

3.3 | The proposed ALE model

The proposed model is an model, which is based on grids like the one described in the preceding section. The discretization can be done either with finite elements or FD. We have chosen the latter. The complete equation describing the evolution of excess pore pressure is now written as:

$$\begin{aligned}\frac{\partial \Delta p_w}{\partial t} + e_R\left(1-\frac{x_3}{h}\right)\frac{\partial \Delta p_w}{\partial x_3} &= -\rho' b_3 \frac{d^{(s)}h}{dt}\left(1-\frac{x_3}{h}\right)\\ &+ \frac{K_v}{\alpha}\frac{\partial}{\partial x_3}\left(\frac{\bar{n}}{\bar{C}_d}\frac{\partial \Delta p_w}{\partial x_3}\right) - \frac{K_v}{\alpha}\frac{1}{1-\bar{n}}\frac{d^{(s)}\bar{n}}{dt}\end{aligned} \tag{38}$$

where we have advection, diffusion and source terms. The equation is of the type

$$\frac{\partial \phi}{\partial t} + A\frac{\partial \phi}{\partial x} = D\frac{\partial^2 \phi}{\partial x^2} + S \tag{39}$$

where S includes now all source terms.

We will solve the equation using a fractional step method:

$$\begin{aligned}\frac{\phi^* - \phi^n}{\Delta t} &= -A\phi_x|^n\\ \frac{\phi^{n+1} - \phi^*}{\Delta t} &= D\phi_{xx}|^n + S|^n\end{aligned} \tag{40}$$

Regarding the advection step, explicit centered schemes (FE and FD) are unconditionally unstable. A convenient solution is to use either:

i. a FE Taylor Galerkin scheme (Lohner et al.,[48] and Donea[49]) or
ii. a FD Lax-Wendroff scheme (Smith,[50] and Hirsch[51]), which is the simple method we will use here, because of its speed.

The time step length is limited by the Courant-Friedrichs-Lewy condition (Courant number) should be smaller or equal than 1:

$$\Delta t \leq \frac{\Delta x}{A} \tag{41}$$

Taking into account that:

$$\max(A) = \max(e_R(1 - x/h)) = e_R \tag{42}$$

the limit results on:

$$\Delta t \leq \frac{\Delta x}{e_R} \tag{43}$$

Regarding the diffusion step, the limitation of the explicit central scheme is:

$$\Delta t \leq \frac{\Delta x^2}{2C_v} \tag{44}$$

If source terms are dominant, a time step limitation should be used. The increment of time should be selected as the minimum of them. Computations of excess pore pressure performed at all SPH nodes of the solid fraction and at all SPH time steps, which leads to sub stepping on Δt_{SPH}.

As the equation has a parabolic component, boundary conditions are required at both ends. In this Stefan problem:

i. At the surface, we assume that excess pore pressure is zero.
ii. At the bottom, we prescribe an excess pore pressure $\Delta p_{w\,b}$ which should be that of the underlying soil which is being eroded.

Regarding this boundary condition, depth integrated models have to make an extra assumption, as no information on the stresses in the basal material is available. Here, using a 3D model such as the one proposed by Crosta et al.[14] will circumvent this limitation at the cost of performing an expensive 3D, coupled, non linear computation.

Initial conditions of the landslide have to be assumed too. For instance, full liquefaction of the landslide, either on the whole mass or in a layer close to the bottom. Again, 3D models are the only way of knowing the initial conditions accurately.

3.4 | Time scales for consolidation and erosion

The behaviour of the pore pressure in the landslide body depends on the relative influence of the convection and diffusion terms. To gain some insight on this issue, we will consider the non dimensional form of the convection-diffusion equation without sources. For simplicity, we will use the reference system sketched in Figure 4, we will denote $p = \Delta p_w$ and we will not include the source terms.

$$\frac{\partial p}{\partial t} + e_R\left(1 - \frac{x}{h}\right)\frac{\partial p}{\partial x} = C_v \frac{\partial^2 p}{\partial x^2} \tag{45}$$

We will define the following non dimensional magnitudes:

i. $\widehat{x} = x/h_0$ where h_0 is the initial height of the column.
ii. $\widehat{t} = t/T_c$ where T_c is the consolidation time $T_c = h_0^2/C_v$.

iii. $\widehat{p} = p/\rho_w g h_0$ After substituting in the equation, we arrive to:

$$\frac{\partial \hat{p}}{\partial t} + \frac{e_R T_c}{h_0}\left(1 - \frac{\hat{x}}{\hat{h}}\right)\frac{\partial \hat{p}}{\partial \hat{x}} = \frac{\partial^2 \hat{p}}{\partial \hat{x}^2} \tag{46}$$

We will define next a characteristic erosion time:

$$T_e = h_0/e_R \tag{47}$$

from where we obtain:

$$\frac{\partial \hat{p}}{\partial t} + \frac{T_c}{T_e}\left(1 - \frac{\hat{x}}{\hat{h}}\right)\frac{\partial \hat{p}}{\partial \hat{x}} = \frac{\partial^2 \hat{p}}{\partial \hat{x}^2} \quad 0 \le \hat{x} \le \hat{h}(t) \tag{48}$$

with $\hat{h}(t) = 1 + \frac{T_c}{T_e}\hat{t}$.

The boundary conditions will be:

$$\begin{aligned} \hat{p} &= 0 \quad \hat{x} = 1 \\ \hat{p} &= \hat{p}_b \quad \hat{x} = 0 \end{aligned} \tag{49}$$

complemented by the initial condition.

If this non dimensional equation is to be solved using a Lax Wendroff scheme, the stability condition will be:

$$\Delta \hat{t} \le \min\left(\frac{\Delta \hat{x}}{T_c/T_e}, \frac{\Delta \hat{x}^2}{2}\right) \tag{50}$$

The Péclet number characterizing the predominant behaviour is therefore:

$$Pe = \frac{T_c}{T_e}\left(1 - \frac{\hat{x}}{\hat{h}}\right) \le \frac{T_c}{T_e} \tag{51}$$

We can see that Pe varies linearly along the depth, being 0 at the surface and Tc/Te at the bottom.

Large Péclet numbers (consolidation times larger than erosion time) indicate convection dominated problems, while $T_c << T_e$ will show diffusion dominated problems.

3.5 | The pure convection problem

In order to study the asymptotic behaviour when $P_e \to \infty$, we will use for convenience a modification in our reference system, defining a new abscissa and measured from the top, where it is zero, to the bottom, where its value is $h(t)$, as depicted in Figure 5. It is defined as:

$$y = h(t) - x \tag{52}$$

We will not use the consolidation time but the erosion time to define the non-dimensional time:

$$\hat{t} = \frac{t}{T_e} = \frac{t\, h_0}{e_R} \tag{53}$$

The non dimensional equation is:

$$\frac{\partial \hat{p}}{\partial \hat{t}} - \frac{\hat{y}}{\hat{h}}\frac{\partial \hat{p}}{\partial \hat{y}} = 0 \qquad 0 \le \hat{y} \le \hat{h}(t) \tag{54}$$

with $\hat{h}(t) = 1 + \hat{t}$.

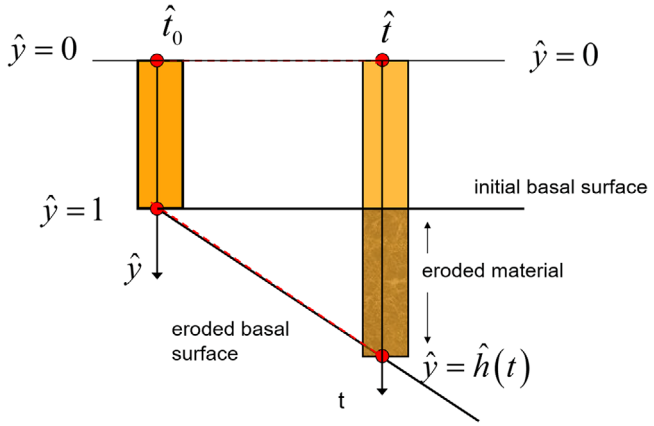

FIGURE 5 Coordinates for the pure advection problem

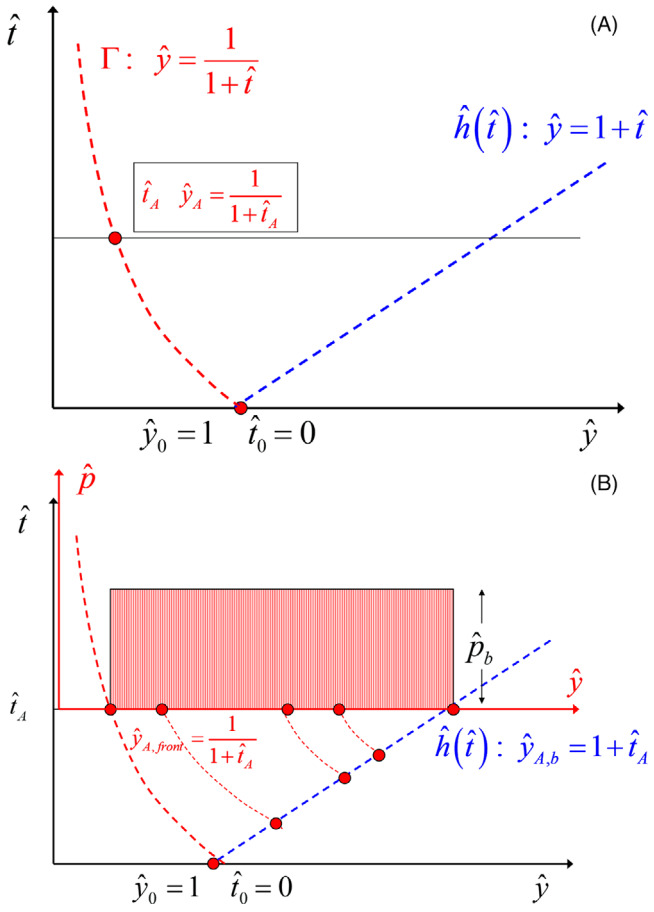

FIGURE 6 (A) Propagating front. (B) Characteristics and values of the pressure at a given time $\hat{t}_A$

The boundary condition (only at the bottom) will be:

$$\hat{p}=\hat{p}_b \quad \hat{y}=1 \quad (bottom) \tag{55}$$

complemented by the initial condition.

This PDE is a scalar linear hyperbolic equation, for which characteristic lines provide interesting information. The solution of the problem (see Farlow[52]) is obtained in two steps. First, the characteristic lines Γ are obtained. Along them, the PDE is transformed into an ODE, which can be integrated much easily.

Here, the characteristic lines are:

$$\Gamma: \quad \frac{d\hat{y}}{d\hat{t}} = -\frac{\hat{y}}{\hat{h}(\hat{t})} = -\frac{\hat{y}}{1+\hat{t}} \tag{56}$$

and along them, the non dimensional pressure is constant. They can be easily integrated, resulting on:

$$\hat{y} = \hat{y}_0\left(\frac{1+\hat{t}_0}{1+\hat{t}}\right) \tag{57}$$

where $(\hat{t}_0, \hat{y}_0)$ is a point of the characteristic where we know the solution (usually by the initial or the boundary condition).

Let us consider the case where the boundary initial condition is zero in the whole domain and the boundary condition at the bottom is $\hat{p} = \hat{p}_b$. We will consider the characteristic entering the domain at $(\hat{y}_0 = \hat{h}_0 = 1\,,\ \ \hat{t}_0 = 0)$ which is given by:

$$\hat{y} = \left(\frac{1}{1+\hat{t}}\right) \tag{58}$$

The solution, as illustrated in Figure 6, consists of a front propagating from the bottom along above defined characteristic line.

4 | APPLICATIONS

The purpose of this section is to present two examples which will be used to assess how the proposed model performs, comparing it to other simpler models -which are special cases of the general model proposed here. The selected cases are a simple theoretical 1D problem and a real debris flow which happened in Hong Kong in 1999.

4.1 | A simple advection-diffusion example: Influence of Péclet number

In order to illustrate the properties of the model being solved, we will consider next some properties of the advection-diffusion non dimensional problem given in Equation 48 with different Péclet numbers.

The first case consists of a problem with a Péclet number of 10, that is, an advection dominated problem. The bottom is located at the left, $\hat{x} = 0$. Boundary conditions are $\hat{p} = \hat{p}_b = 1$ at the bottom and $\hat{p} = 0$ at the top of the column. At time zero, pressure is set to zero. We will assume that the erosion velocity e_R is constant.

We have depicted in Figure 7 the non dimensional pore pressure evolution for non dimensional times $\hat{t} = \{0.01, 0.05, 0.10, 0.50, 1.0, 5.0\}$ We can see how, as time increases, a the profile is steepening, approaching a constant distribution of pressure which becomes zero at the right boundary $\hat{p} = (1 - \delta(1-x))$ where the delta distribution $\delta(1-x)$ is zero everywhere except at point 1.

The second case consists of the same problem, where we have assumed a Péclet number of 001, that is, a diffusion dominated problem. Again, boundary conditions are $\hat{p} = \hat{p}_b = 1$ at the bottom and $\hat{p} = 0$ at the top of the column. At time zero, pressure is set to zero. The results are shown in Figure 8, where we can see how the pore pressure distribution reaches the analytical solution for the pure diffusive problem at a time 0.5, which is the linear profile $\hat{p} = 1 - \hat{x}$.

Cases with intermediate Péclet numbers will exhibit a combination of advective and diffusive behaviours, as shown in Figure 9.

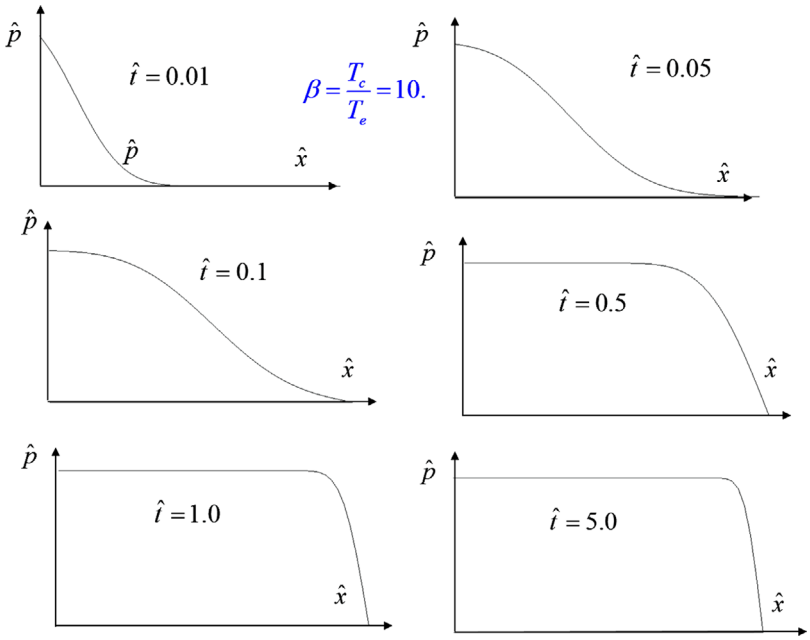

FIGURE 7 Pore pressure evolution in an advection dominated problem

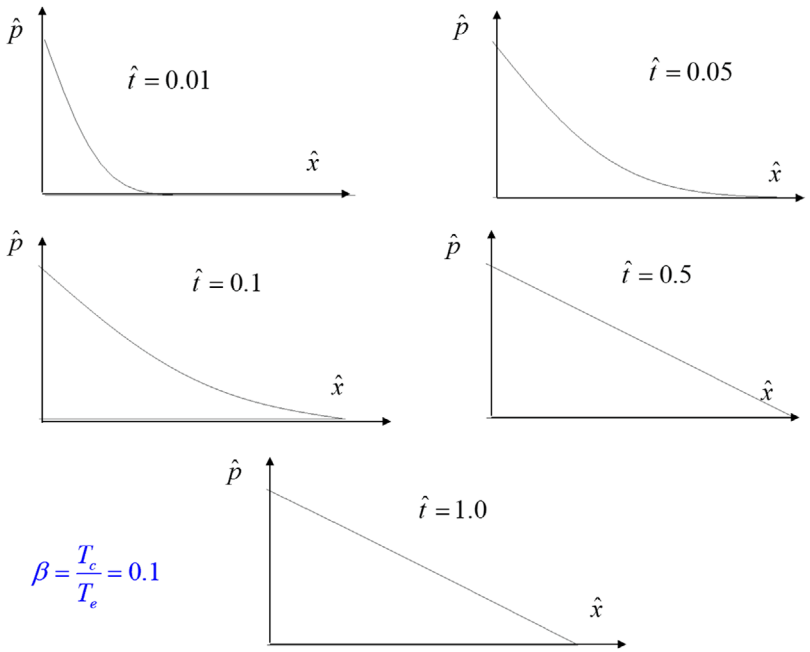

FIGURE 8 Pore pressure evolution for a diffusion dominated problem

4.2 | Tsing Shan debris flow (Hong Kong, 1990)

4.2.1 | Description

Once we have seen how the relative stress of advective and diffusive terms influences the behaviour, we will analyze a practical case, the Tsing Shan debris flow which happened in Hong Kong in 1990. There was a significant basal erosion, and this is the reason to choose this case. As stated before, we are not proposing any erosion model, which is a subject of active research today. In our opinion, basal pore pressures combined with erosion may affect in a significant manner property as runout of debris flows and other similar phenomena.

Indeed, the purpose of this exercise is to compare two different approaches for modelling of entrainment processes where excess pore pressures exist in the entrained material. The classic approach is what was proposed in Pastor et al.[5] There, height of the column increased at every time step with the eroded material, but the formulation did not take into

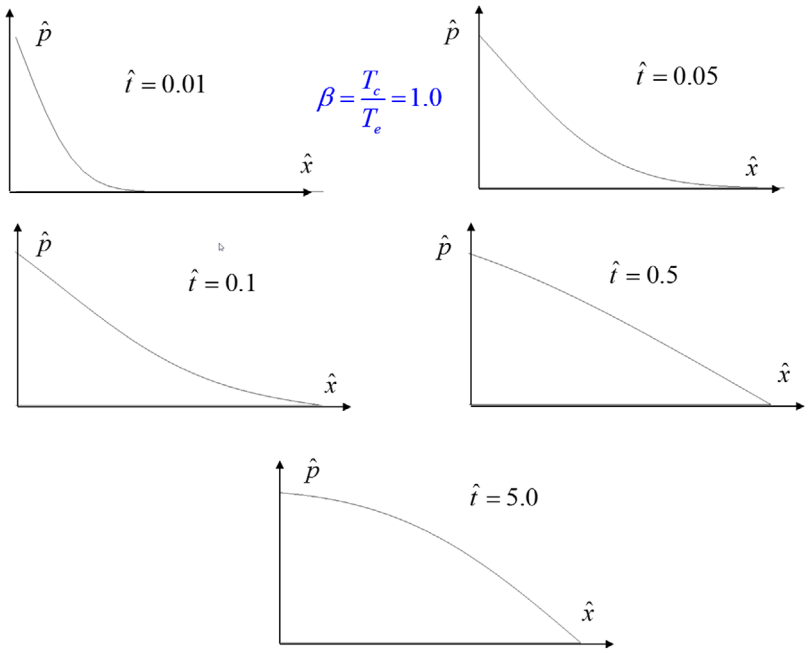

FIGURE 9 Pore pressure evolution for a convective-diffusive problem (Péclet number = 1)

FIGURE 10 Oblique view of the debris flow (Hong Kong Geotechnical Office)

account the advection of the entrained material into the FD mesh. Therefore, our goal consists of presenting situations where not using the ALE formulation we propose here results in smaller runouts, predicting smaller risks.

The case we will be analyzing here is a small sized debris flow which happened in Hong Kong in 1990. It was proposed as a benchmark test by the Hong Kong Geotechnical Office for a benchmarking exercise aiming to assess the accuracy of existing models. The activity was part of the 2007 International Forum on Landslide Disaster Management.[53] A group of invited teams was provided digital terrain elevation maps, including both the final terrain surface and the sliding mass, together with the report of Fugro Maunsell Scott Wilson Joint Venture, FMSWJV)[54] on this particular debris flow.

Figure 10, kindly provided by Hong Kong Geotechnical Engineering Office, depicts an aerial oblique view of the debris flow, while Figure 11 shows the deposition area.

FIGURE 11 Oblique view of deposition area (King)[55]

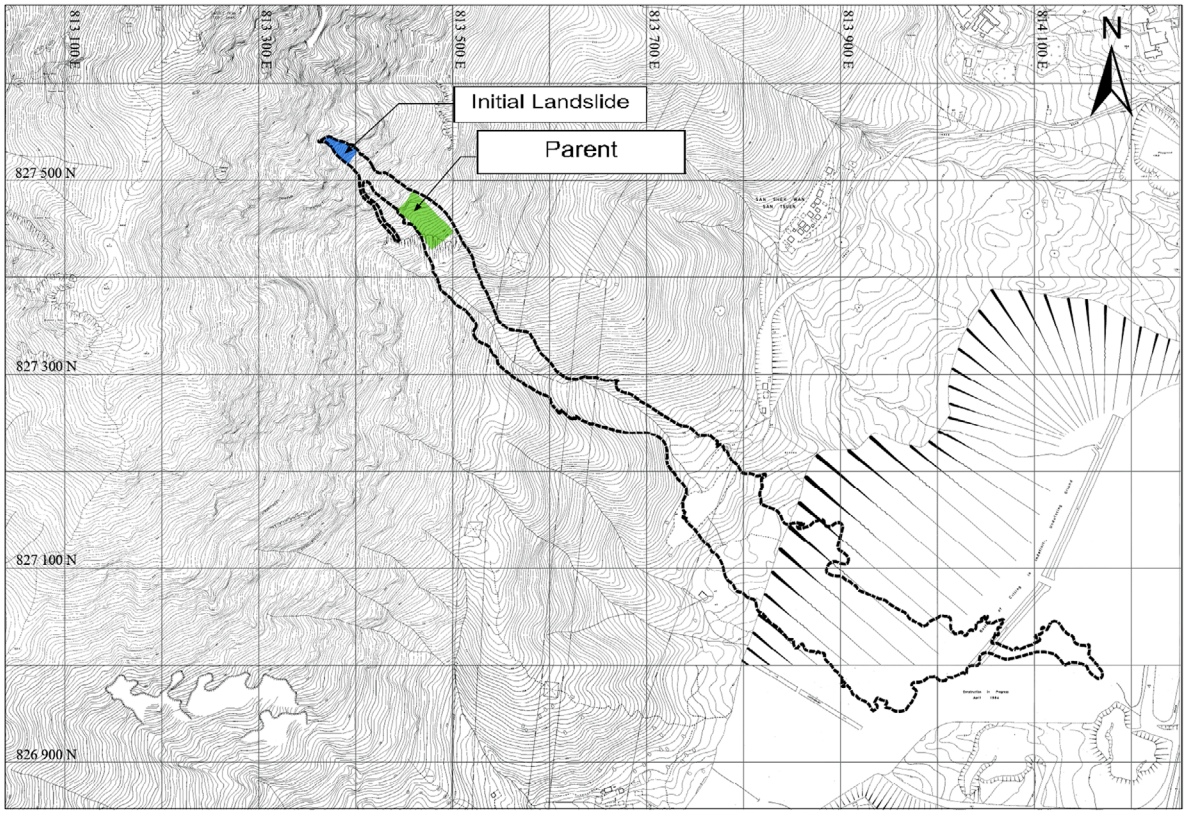

FIGURE 12 Position of initial and parent landslides (King)[55]

This debris flow involved two masses, depicted in Figure 12, referred to as 'trigger or initial' and 'parent', with initial volumes estimated as 350 and 2000 cubic meters. The former traveled downhill, hitting the latter mass and triggering its movement.

The report states that *'…the loose condition of the displaced material and the presence of sufficient fines in it to reduce permeability allowing slurry flow…' and '… As the debris travelled downslope along a drainage line, significant entrainment of the loose bouldery colluvium that was present at the drainage line occurred. This escalated the debris volume, and the final volume of the event is about 20,000 m3 with a travel angle of about 26° to the distal edge of the primary deposition zone'.*

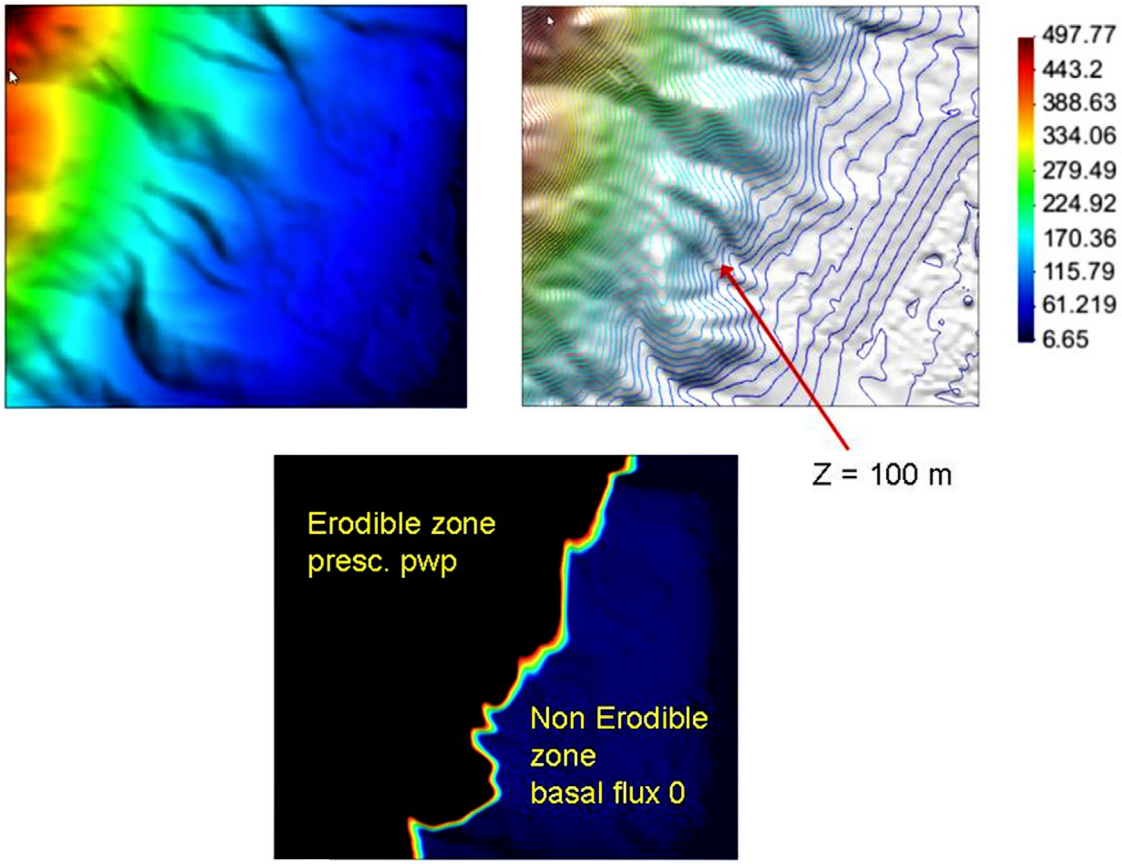

FIGURE 13 Erodible and non-erodible zones

Regarding the triggering mechanism of the initial mass, it was caused by the rainstorm, which produced a raise in the water table *'resulting in saturation of the deposit and decrease in effective stress leading to sliding. If very high pore pressures were generated due to the presence of soil pipes a possible mechanism would be insitu liquefaction of the colluvium'.*

4.2.2 | Modelling method and assumptions

The digital elevation model was provided by Hong Kong Geotechnical Office to participants on the 2007 Benchmarking Activity.[53] Elevations were given on a 5 m uniformly spaced grid. Data of both the initial and parent landslides was given on the same grid. From there, we have obtained the ASCII files used by our models (GeoFlow-SPH). We have approximated the initial conditions at the time at which the initial landslide hits the parent mass, assuming both at rest.

Regarding initial pore water distribution, we have assumed that a basal layer of a thickness equal to one tenth of the height had developed an excess pore water pressure equal to 0.65 times the liquefaction value.

For the entrained material, the model can assume an initial excess pore water pressure, which is applied as a boundary condition at the bottom. As the problem involves a diffusive part (second order spatial derivatives), we need to impose a boundary condition at the top, which is zero, as it is at the atmospheric pressure.

The boundary condition at the bottom will change when crossing a non erodible zone. There, a no-flow condition will be imposed, and the advective terms will be zero. In this case, we have assumed that below an elevation of 100 m, no erosion takes place. This is illustrated in Figure 13.

Regarding material properties of the flowing material, the permeability of the debris was estimated for the deposit as $9 - 23 \times 10^{-6}\ m/s$, from which we have chosen a value of the coefficient of consolidation of $Cv = 0.0004\, m^2/s$ and a basal friction angle of 32° with $\tan\phi = 0.6$.

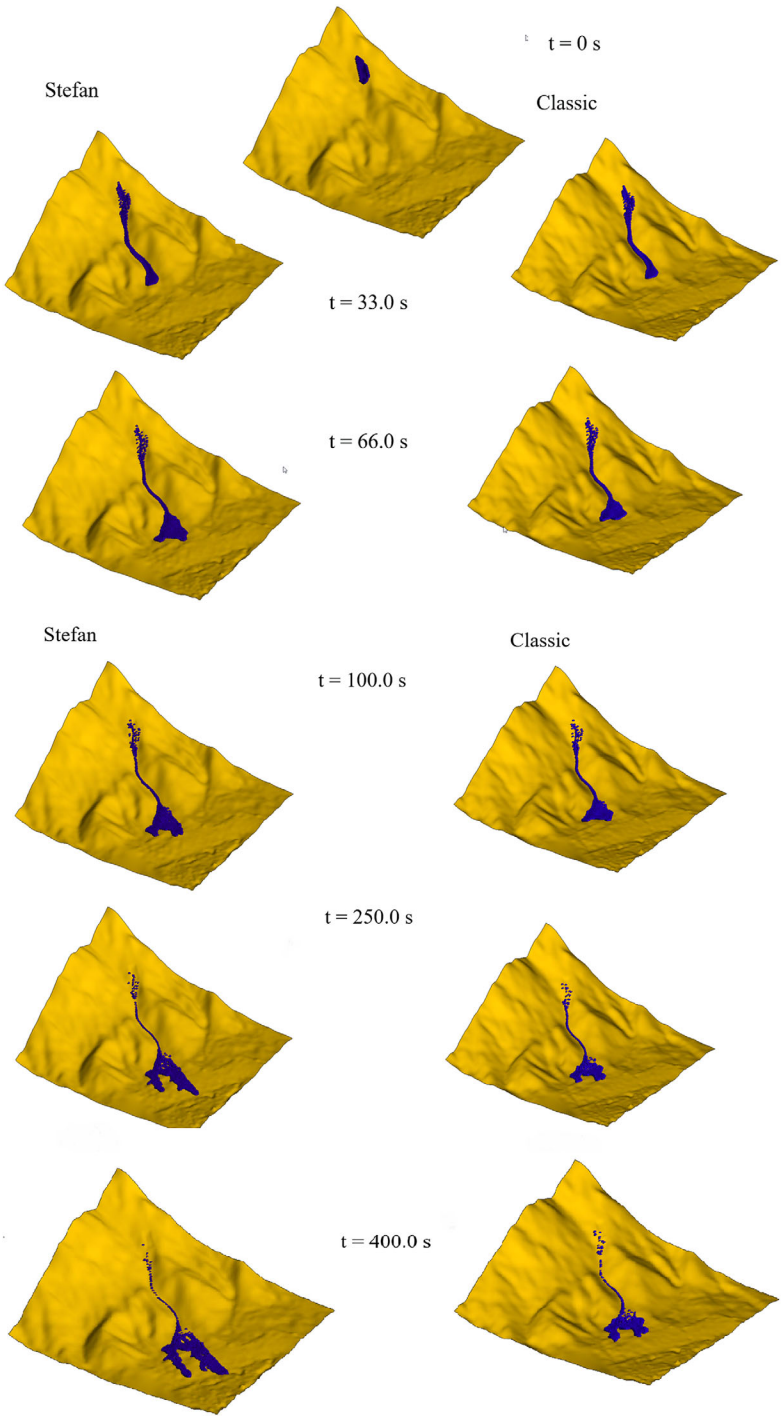

FIGURE 14 Position of the debris flow at times 0, 33, 66, 100, 250 and 400 s. Proposed Arbitrary Lagrangian Eulerian (ALE) method (left) and classical approach (right)

The rheological model is that proposed by Pastor et al.[5] We have assumed that there exists basal slip, with a basal value of the velocity equal to 0.2 times that of the surface. The model includes a linear viscosity term, which has been chosen as $0.5 Pa.s$. Erosion has been modelled using the simple Hungr's law, for which a coefficient of $3\,e-3\ m^{-1}$ has been chosen.

4.2.3 | Results

With the set of material properties and initial and boundary conditions described, we have found longer runouts when using the corrected ALE approach. We will start by considering the propagation of the debris flow and the final runout. This is depicted in Figure 14, where we have plotted the position of the SPH nodes at times 0, 33, 66, 100, 250 and 400 s.

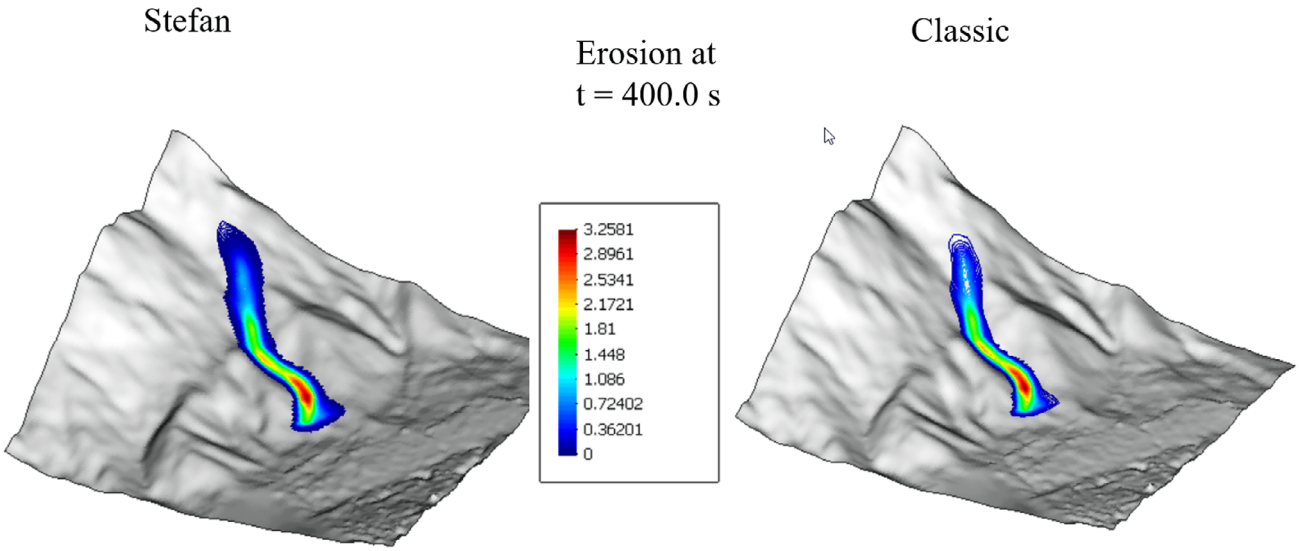

FIGURE 15 Debris flow eroded depths at time 400 s. Proposed Arbitrary Lagrangian Eulerian framework (ALE) method (left) and classical approach (right)

We can see how the runout is larger with the proposed approach. It is important to notice that during the time where erosion takes place, both approaches yield the same nodal displacements. Changes start at the 100 m elevation isoline. Figure 15 presents the eroded depth at the final time of 400 s. We can see how erosion has only taken place above the 100 m elevation isoline, the results being the same in both approaches.

As the eroded material is the same, it is logical to expect that depth of the deposits will be higher in the classical approach, where the deposit is more concentrated. This can be seen in Figure 16, where we have plotted the depth isolines flow at times 0, 32, 66, 150, 250 and 400 s.

The difference in the observed behavior comes from the excess pore pressure distribution along depth. We will illustrate this by using the profiles at a particular node (1468 in our analysis), for which we provide the excess pore water pressures at 32 and 160 s in Figure 17.

At time 32 s, node 1468 is still in the erosion zone. This means that basal pore pressures (relative to liquefaction) are the same. Note that advection of the basal pore pressure has generated much higher pressures inside the column, and this will be responsible for the much lower basal pressures of the classical approach.

The strength of this effect depends on the relative values of the consolidation and the erosion times, characterized by the basal Péclet number. We present in Figure 18 the isolines of the basal Péclet number at time 40, with values much higher than unity.

One important question is how we could assess the importance of using the proposed approach. In our opinion, the key is the Péclet number. We will repeat the analysis using a much smaller coefficient of consolidation ($0.4\,m^2/s$) for which the consolidation time decreases by a factor of 1000. As erosion time will not change much -indeed the eroded amount of material is the same- we will be reducing the Péclet number to values close to 0.3. Dissipation of excess pore pressures will be faster, resulting on very similar runouts and height of deposits.

We plot in Figure 19 the final position of SPH nodes and the contours of basal excess pore pressures, the depth of the final deposit being plotted in Figure 20. Figure 21 shows the profiles of excess pore pressure at node 1468 at times 32 and 160 s.

Looking at the contours plotted in Figure 22 for t = 32 s, we can see how the pwp distribution has almost reached the equilibrium when boundary conditions are at the base and the surface, respectively, 0.65 and 0. Indeed, the time of consolidation can be estimated as $T_v \approx \frac{h^2}{C_v} \approx \frac{10}{0.4} = 25s$ with a Péclet number close to 0.4, which indicates a diffusion driven problem. We can see how, in this case, the results of both the classical and the Stefan based approach are almost the same.

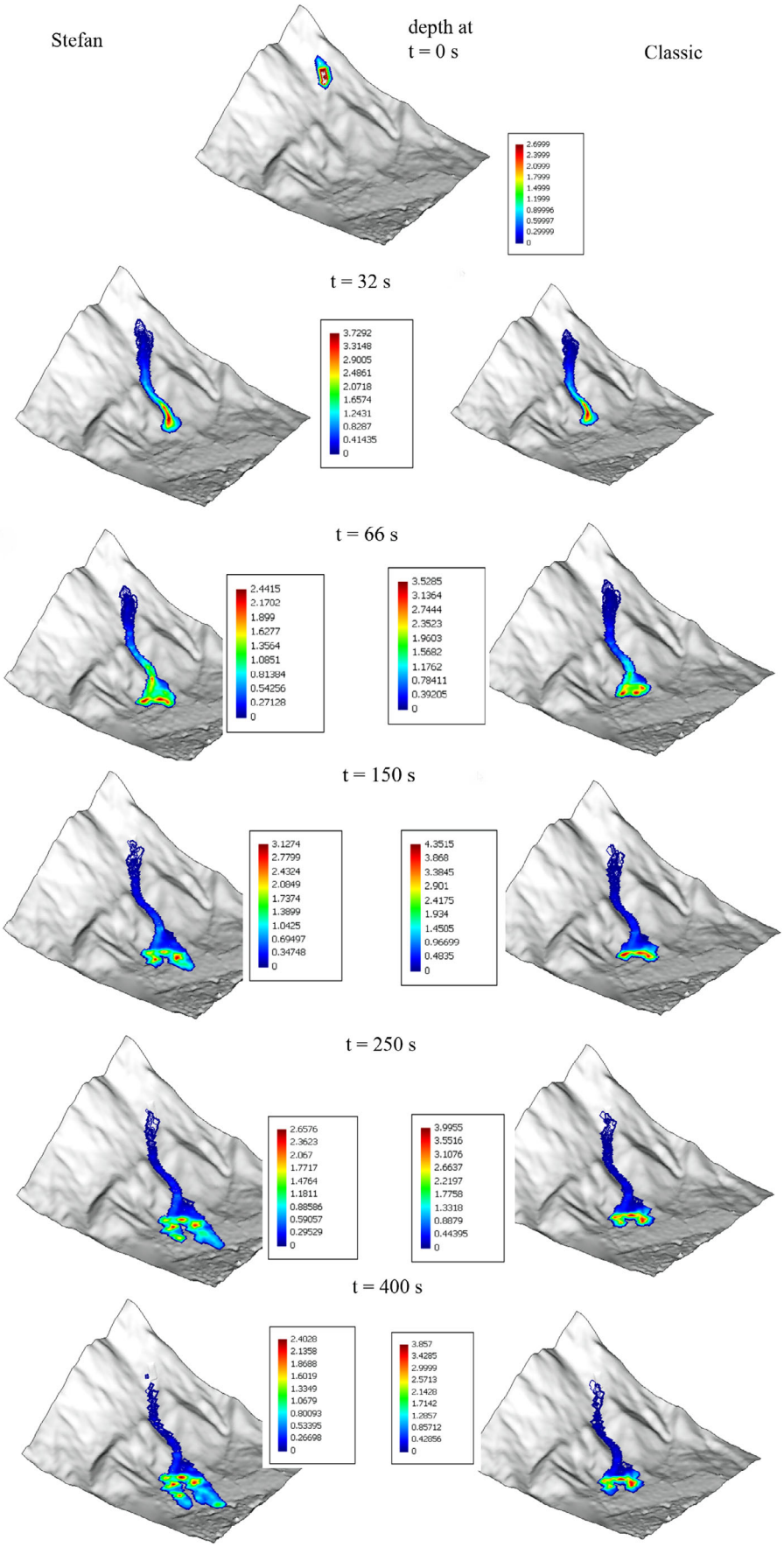

FIGURE 16 Debris flow depths at times 0, 32, 66, 150, 250 and 400 s. Proposed Arbitrary Lagrangian Eulerian (ALE) method (left) and classical approach (right)

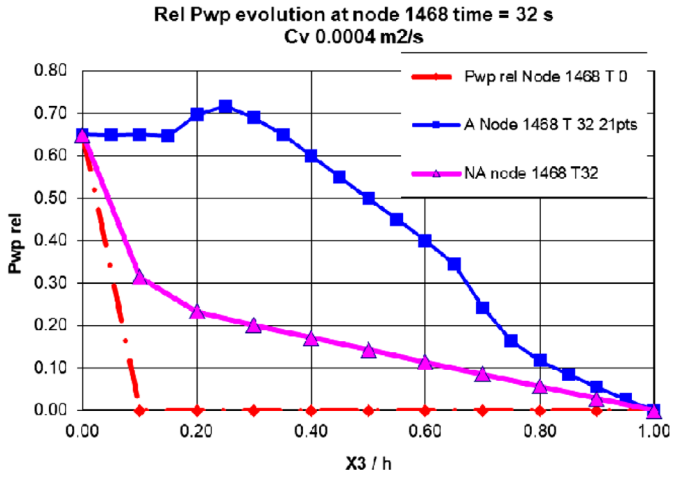

FIGURE 17 Excess pore pressure profiles at times 32 and 160 s. Proposed ALE method and classical approach

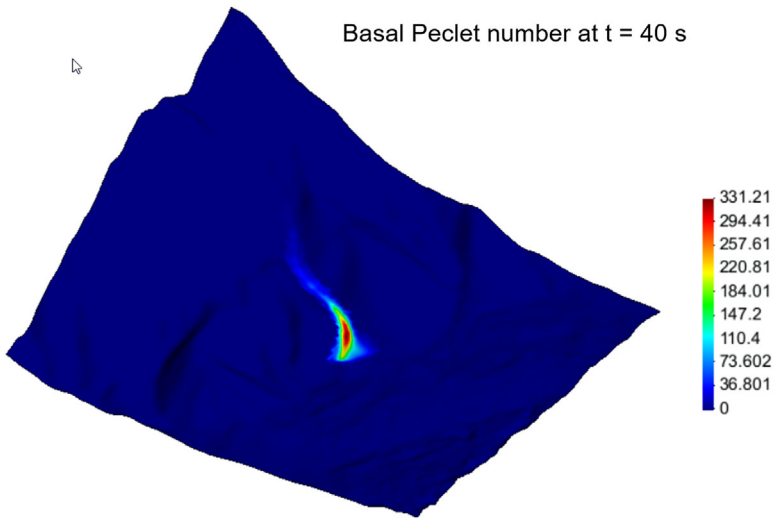

FIGURE 18 Isolines of basal Péclet number at time 40 s

5 | CONCLUSIONS

The entrainment of saturated bed material may increase the mobility of fast landslides, because of the modification induced on the excess pore pressure profiles. The problem is difficult to model using depth integrated models where the distribution along depth of the main magnitudes, such as the excess pore pressure, has been lost unless special

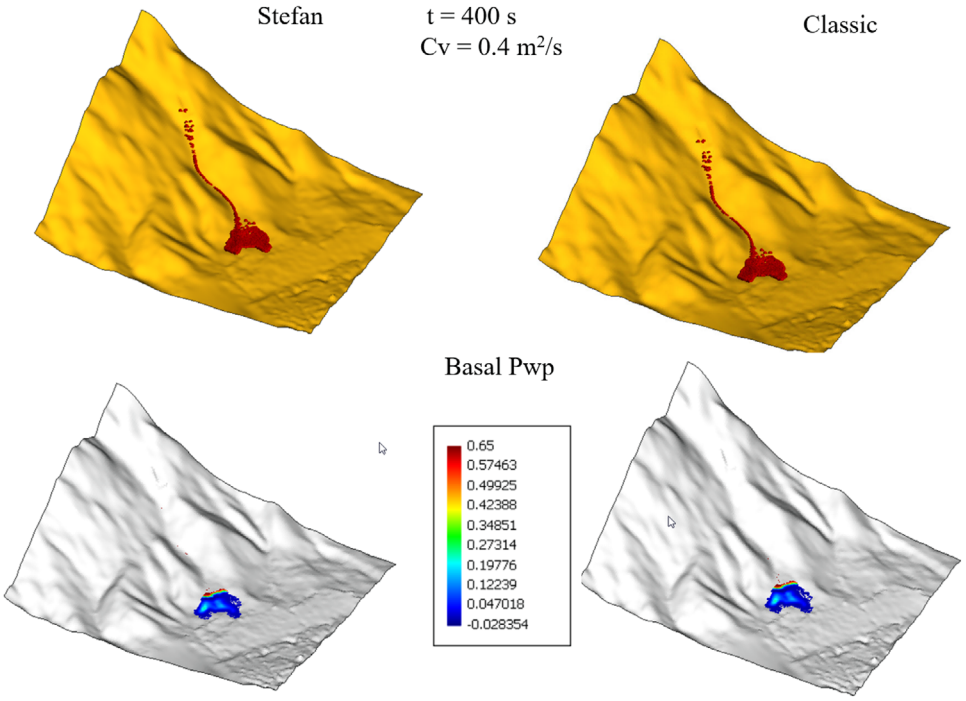

FIGURE 19 Final position of SPH nodes and contours of basal pore pressures at time 400 s

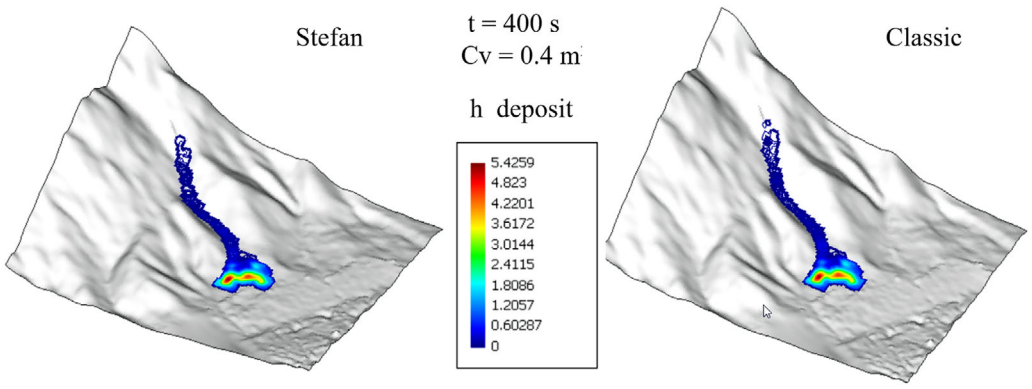

FIGURE 20 Contours of depth at time 400 s

techniques such as FD meshes implementation at SPH nodes are used. This technique, introduced by the author (Pastor et al.), has proven useful for cases where no entrainment of saturated materials with their associated pore pressures exists. In order to circumvent this limitation in those cases where it is important, we have proposed solving the Stefan problem (with a moving boundary at the bottom) using an ALE formulation. We have presented a non dimensional formulation of a simplified version of the problem, from which we have found that a non dimensional number, the basal entrainment Péclet number indicates when the proposed formulation will be necessary. The paper presents a practical case where we compare the classical formulation with the ALE based model.

We would like to point out finally the importance of knowing the conditions at which the erodible base is. To accurately describe it, it is necessary to use models where the conditions imposed by the pass of the landslide can be reproduced, obtaining the pore pressure induced at the bed. Here, we have assumed that the pore pressures at the bed were known, imposing them as a boundary condition in the Stefan problem. The erosion rate is given by the Hungr formula (McDougall and Hungr).[20] We are aware that the complete solution will come from full 3D models such as those proposed by Crosta et al.[14] or Nikooei and Manzari).[15]

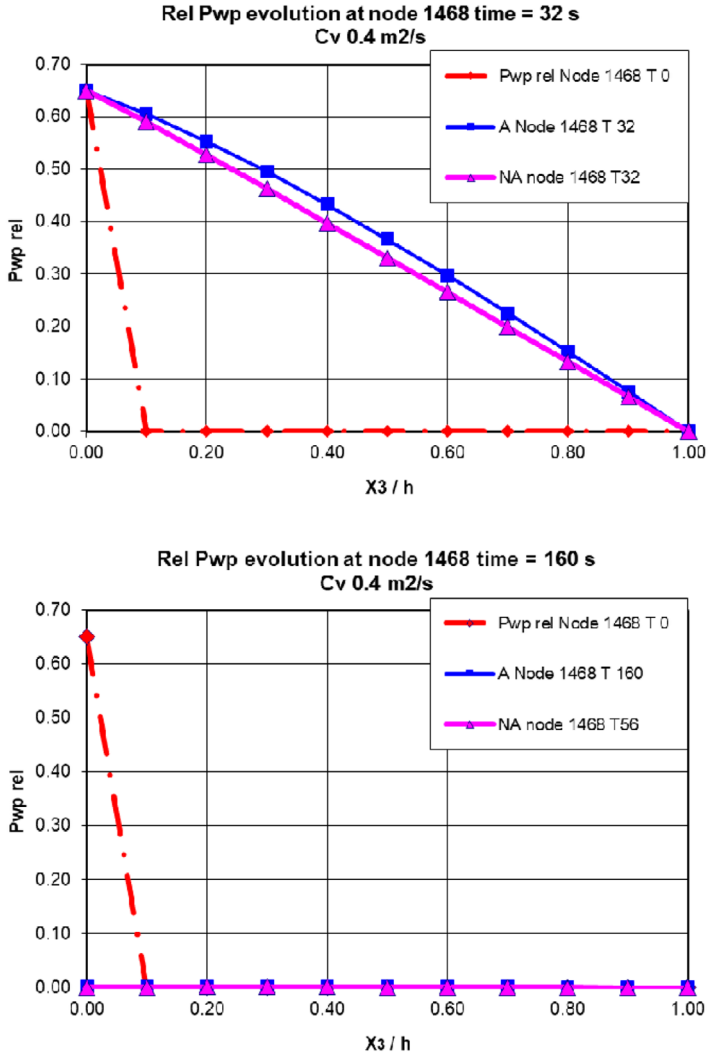

FIGURE 21 Profiles of excess pore pressure at node 1468 at times 32 and 160 s (A Stefan based approach NA classic model)

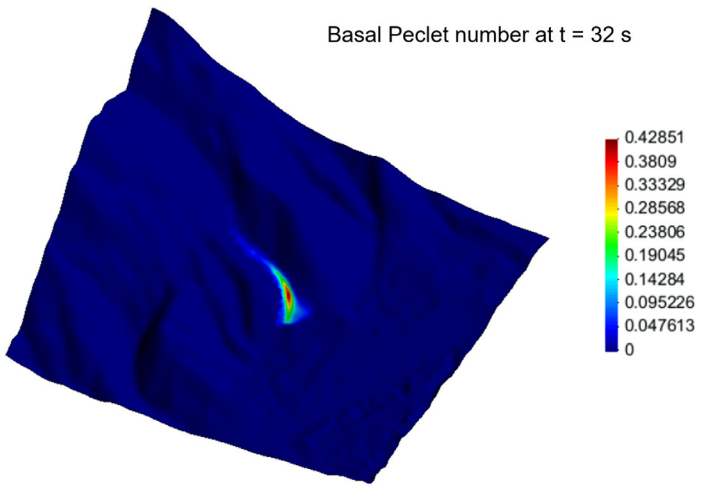

FIGURE 22 Basal Péclet number at t = 32 s when $Cv = 0.4\, m^2/s$

ACKNOWLEDGEMENTS

The authors gratefully acknowledge the economic support provided by the Spanish Ministry MINECO under project P-LAND (PID2019-105630GB-I00). In addition, the authors gratefully acknowledge the support of the Geotechnical Engineering Office, Civil Engineering and Development Department of the Government of the Hong Kong SAR in the provision of the digital terrain models for the Hong Kong landslide case.

FINANCIAL DISCLOSURE
None reported.

CONFLICT OF INTEREST
The authors declare no potential conflict of interests.

DATA AVAILABILITY STATEMENT
The authors declare that the data supporting the findings of this study are available within the article.

ORCID
Manuel Pastor https://orcid.org/0000-0001-8080-0013
Saeid M. Tayyebi https://orcid.org/0000-0002-1980-5963
Miguel M. Stickle https://orcid.org/0000-0001-7591-418X
Miguel Molinos https://orcid.org/0000-0002-5073-4796
Angel Yague https://orcid.org/0000-0002-3290-9433
Diego Manzanal https://orcid.org/0000-0002-6087-3255
Pedro Navas https://orcid.org/0000-0002-0482-378X

REFERENCES
1. Hutchinson JN, Bhandari RK. Undrained loading, a fundamental mechanism of mudflows and other mass movements. *Géotechnique*. 1971;21(4):353–358. https://doi.org/10.1680/geot.1971.21.4.353
2. Hutchinson JN. A sliding-consolidation model for flow slides. *Can Geotech J*. 1986;23(2):115–126. https://doi.org/10.1139/t86-021
3. Iverson RM. The physics of debris flows. *Rev Geophys*. 1997;35(3):245–296. https://doi.org/10.1029/97RG00426
4. Iverson RM, Denlinger RP. Flow of variably fluidized granular masses across three-dimensional terrain: 1. Coulomb mixture theory. *J Geophys Res Solid Earth*. 2001;106(B1):537–552. https://doi.org/10.1029/2000JB900329
5. Pastor M, Blanc T, Haddad B, et al. Depth averaged models for fast landslide propagation: mathematical, rheological and numerical aspects. *Arch Comput Methods Eng*. 2015;22(1):67–104. https://doi.org/10.1007/s11831-014-9110-3
6. Pastor M, Tayyebi S, Stickle M, et al. A depth integrated, coupled, two-phase model for debris flow propagation. *Acta Geotech*. 2021:1–25. https://doi.org/10.1007/s11440-020-01114-4
7. Abele G. Rockslide movement supported by the mobilization of groundwater-saturated valley floor sediments. *Zeitschrift für Geomorphol*. 1997;41(1):1–20. https://doi.org/10.1127/zfg/41/1997/1
8. Sassa K *The mechanism of debris flows*. In: 1985; San Francisco: Rotterdam; Boston; 1173–1176.
9. Sassa K, Wang hG. *Mechanism of Landslide-Triggered Debris Flows: Liquefaction Phenomena due to the Undrained Loading of Torrent Deposits*. Berlin, Heidelberg: Springer Berlin Heidelberg; 2005:81–104.
10. Iverson RM, Reid ME, Logan M, LaHusen RG, Godt JW, Griswold JP. Positive feedback and momentum growth during debris-flow entrainment of wet bed sediment. *Nat Geosci*. 2011;4(2):116–121. https://doi.org/10.1038/ngeo1040
11. Iverson RM. Elementary theory of bed-sediment entrainment by debris flows and avalanches. *J Geophys Res Earth Surf*. 2012;117(F3):n/a–n/a. C8: F03006. https://doi.org/10.1029/2011JF002189
12. Lê L, Pitman EB. A model for granular flows over an erodible surface. *SIAM J Appl Math*. 2010;70(5):1407–1427. https://doi.org/10.1137/060677501
13. Pudasaini SP, Fischer JT. A mechanical erosion model for two-phase mass flows. *Int J Multiph Flow*. 2020;132:103416. https://doi.org/10.1016/j.ijmultiphaseflow.2020.103416
14. Crosta G, Imposimato S, Roddeman D. Numerical modelling of entrainment/deposition in rock and debris-avalanches. *Eng Geol*. 2009;109(1-2):135–145. https://doi.org/10.1016/j.enggeo.2008.10.004
15. Nikooei M, Manzari MT. Investigating the effect of mixing layer rheology on granular flow over entrainable beds using SPH method. *Comput Geosci*. 2021;155:104792. https://doi.org/10.1016/j.cageo.2021.104792
16. Takahashi T. *Debris Flow*. IAHR Monograph Series, A.A. Balkema; 1991.
17. Egashira S, Honda N, Itoh T. Experimental study on the entrainment of bed material into debris flow. *Phys. Chem Earth, Part C Solar, Terr Planet Sci*. 2001;26(9):645–650. https://doi.org/10.1016/S1464-1917(01)00062-9
18. FRACCAROLLO L, CAPART H. Riemann wave description of erosional dam-break flows. *J Fluid Mech*. 2002;461:183–228. https://doi.org/10.1017/S0022112002008455
19. Pitman E, Nichita C, Patra A, Bauer A, Bursik M, Webb A. A model of granular flows over an erodible surface. *Discret Contin Dyn Syst - B*. 2003;3(4):589–599. https://doi.org/10.3934/dcdsb.2003.3.589
20. McDougall S, Hungr O. Dynamic modelling of entrainment in rapid landslides. *Can Geotech J*. 2005;42(5):1437–1448. https://doi.org/10.1139/t05-064
21. Issler D, Jóhanesson T & Gauer P *General Considerations and Constraints on Entrainment Mechanisms in Rapid Gravity Mass Flows*. In: 2008; San Francisco, CA; Washington, D.C.

22. Issler D. Dynamically consistent entrainment laws for depth-averaged avalanche models. *J Fluid Mech*. 2014;759:701–738. https://doi.org/10.1017/jfm.2014.584
23. Pastor M, Yague A, Stickle MM, Manzanal D, Mira P. A two-phase SPH model for debris flow propagation. *Int J Numer Anal Methods Geomech*. 2018;42(3):418–448. https://doi.org/10.1002/nag.2748
24. Biot MA. General theory of three-dimensional consolidation. *J Appl Phys*. 1941;12(2):155–164. https://doi.org/10.1063/1.1712886
25. Zienkiewicz OC, Shiomi T. Dynamic behaviour of saturated porous media; the generalized Biot formulation and its numerical solution. *Int J Numer Anal Methods Geomech*. 1984;8(1):71–96. https://doi.org/10.1002/nag.1610080106
26. Anderson TB, Jackson R. Fluid mechanical description of fluidized beds. Equations of motion. *Ind Eng Chem Fundam*. 1967;6(4):527–539. https://doi.org/10.1021/i160024a007
27. Pitman EB, Le L. A two-fluid model for avalanche and debris flows. *Philos Trans R Soc A Math Phys Eng Sci*. 2005;363(1832):1573–1601. https://doi.org/10.1098/rsta.2005.1596
28. Pudasaini SP. A general two-phase debris flow model. *J Geophys Res Earth Surf*. 2012;117(F3):F03010. https://doi.org/10.1029/2011JF002186
29. Córdoba G, Sheridan MF, Pitman EB. TITAN2F: a pseudo-3-D model of 2-phase debris flows. *Nat Hazards Earth Syst Sci Discuss*. 2015;3(6):3789–3822. https://doi.org/10.5194/nhessd-3-3789-2015
30. Bui HH, Nguyen GD. A coupled fluid-solid SPH approach to modelling flow through deformable porous media. *Int J Solids Struct*. 2017;125:244–264. https://doi.org/10.1016/j.ijsolstr.2017.06.022
31. Saint-Venant A. Theorie du mouvement non permanent des eaux, avec application aux crues des rivieres et a l'introduction de marees dans leurs lits. *Comptes-Rendus l'Académie Des Sci* 1871;73:147–273.
32. Savage SB, Hutter K. The motion of a finite mass of granular material down a rough incline. *J Fluid Mech*. 1989;199:177–215.
33. Savage SB, Hutter K. The dynamics of avalanches of granular materials from initiation to runout. Part I: analysis. *Acta Mech*. 1991;86(1-4):201–223. https://doi.org/10.1007/BF01175958
34. Hutter K, Siegel M, Savage SB, Nohguchi Y. Two-dimensional spreading of a granular avalanche down an inclined plane Part I. theory. *Acta Mech*. 1993;100(1-2):37–68. https://doi.org/10.1007/BF01176861
35. Gray JM, Wieland M, Hutter K. Gravity-driven free surface flow of granular avalanches over complex basal topography. *Proc R Soc London Ser A Math Phys Eng Sci*. 1999;455(1985):1841–1874. https://doi.org/10.1098/rspa.1999.0383
36. Laigle D, Coussot P. Numerical modeling of mudflows. *J Hydraul Eng*. 1997;123(7):617–623. https://doi.org/10.1061/(ASCE)0733-9429(1997)123:7(617)
37. McDougall S, Hungr O. A model for the analysis of rapid landslide motion across three-dimensional terrain. *Can Geotech J*. 2004;41(6):1084–1097. https://doi.org/10.1139/t04-052
38. Pastor M, Quecedo M, Merodo JA, Herrores MI, Gonzalez E, Mira P. Modelling tailings dams and mine waste dumps failures. *Géotechnique*. 2002;52(8):579–591. https://doi.org/10.1680/geot.2002.52.8.579
39. Pastor M, Haddad B, Sorbino G, Cuomo S, Drempetic V. A depth-integrated, coupled SPH model for flow-like landslides and related phenomena. *Int J Numer Anal Methods Geomech*. 2009;33(2):143–172. https://doi.org/10.1002/nag.705
40. Quecedo M, Pastor M, Herreros MI, Fernández Merodo JA. Numerical modelling of the propagation of fast landslides using the finite element method. *Int J Numer Methods Eng*. 2004;59(6):755–794. https://doi.org/10.1002/nme.841
41. Hutter K, Wang Y, Pudasaini SP. The Savage-Hutter avalanche model: how far can it be pushed?. *Philos Trans R Soc A Math Phys Eng Sci*. 2005;363(1832):1507–1528. https://doi.org/10.1098/rsta.2005.1594
42. Pudasaini SP, Hutter K. *Avalanche Dynamics: Dynamics of Rapid Flows of Dense Granular Avalanches*. Berlin, Heidelberg: Springer Berlin Heidelberg; 2007.
43. Tayyebi SM, Pastor M, Yifru AL, Thakur VK, Stickle MM. Two-phase SPH-FD depth integrated model for debris flows: application to basal grid brakes. *Géotechnique* 2021:0(0):1–16. https://doi.org/10.1680/jgeot.21.00080
44. Crank J. *Free and Moving Boundary Problems*. Oxford: Clarendon Press; 1984.
45. Hill J. *One-Dimensional Stefan Problem: An Introduction, Longman Scientific and Technical*; Longman Scientific & Technical; 1987.
46. Issler D, Pastor Pérez M. Interplay of entrainment and rheology in snow avalanches: a numerical study. *Ann Glaciol*. 2011;52(58):143–147. https://doi.org/10.3189/172756411797252031
47. Savovic S, Caldwell J. Numerical solution of Stefan problem with time-dependent boundary conditions by variable space grid method. *Therm Sci*. 2009;13(4):165–174. https://doi.org/10.2298/TSCI0904165S
48. Löhner R, Morgan K, Zienkiewicz OC. The solution of non-linear hyperbolic equation systems by the finite element method. *Int J Numer Methods Fluids*. 1984;4(11):1043–1063. https://doi.org/10.1002/fld.1650041105
49. Donea J. A Taylor-Galerkin method for convective transport problems. *Int J Numer Methods Eng*. 1984;20(1):101–119. https://doi.org/10.1002/nme.1620200108
50. Smith G. *Numerical Solution of Partial Diferential Equations*. Oxford University Press, Open University Set Book; 1978.
51. Hirsch C. *Numerical Computation of Internal & External Flows: Fundamentals of Numerical Discretization*. New York, NY: John Wiley & Sons, Inc.; 1988.
52. Farlow S. *Partial Diferential Equations for Scientists and Engineers*. John Wiley and Sons; 1982.
53. Ho K, Li V. The 2007 International Forum on Landslide Disaster Management. In: 2007; Hong Kong.

54. Wilson FM. Report on the debris flow at Sham Tseng San Tsuen of 23 august 1999. tech. rep., Findings of the investigation. GEO REPORT No. 169, Geotechnical Engineering Office, Civil Engineering and Development Department, The Government of the Hong Kong Special Administrative Region; 2005.
55. King J Tsing Shan Debris Flow and Debris Flood. GEO Report No. 281. tech. rep.; 2013.

How to cite this article: Pastor M, Tayyebi SM, Stickle MM, Molinos M, Yague A, Manzanal D, Navas P. An Arbitrary Lagrangian Eulerian (ALE) finite difference (FD)-SPH depth integrated model for pore pressure evolution on landslides over erodible terrains. *Int J Numer Anal Methods*. 2022;46:1127–1153. https://doi.org/10.1002/nag.3339